Chemical Science

ROYAL SOCIETY OF CHEMISTRY

EDGE ARTICLE

View Article Online
View Journal | View Issue

Cite this: *Chem. Sci.*, 2025, **16**, 10857

All publication charges for this article have been paid for by the Royal Society of Chemistry

Borinine-FLP ring expansion: isolation of eight-membered B–P rings bridged by μ_2 chalcogenide and chloronium ions†

Nathan C. Frey, ‡[a] Samir Kumar Sarkar,‡[a] Diane A. Dickie, [b] Andrew Molino[a] and Robert J. Gilliard, Jr *[a]

Received 13th March 2025
Accepted 10th May 2025

DOI: 10.1039/d5sc02000j

rsc.li/chemical-science

Boron–phosphorus (B–P) frustrated Lewis pairs (FLPs) are an important class of compounds for activating various small molecules. Utilizing the ring expansion reactivity of 9-chloro-9-borafluorene, a borinine-based FLP was synthesized. Various five-membered main-group element heterocycles were obtained *via* the reaction of the FLP with Me_3NO, S_8, and Se. Subsequent reduction of these species yielded the ring-expanded compounds, each featuring bridging B–E–B (E = O, S, Se) bonds. Similarly, halide abstraction from the FLP with $AgNTf_2$ led to the formation of a cationic ring-expanded compound with a bridging B–Cl–B motif. This motif constitutes one of the first examples of a boron-stabilized chloronium ion, as verified using in-depth bonding analysis methods. Mechanistic pathways for the reduction- and halide abstraction-mediated ring expansion reactions are proposed with the aid of density functional theory. Electronic structure computations were performed to determine the best representation of bonding interactions in each compound, suggesting phosphorus(V)–chalcogen double bonding and chalcogen–boron(III) dative interactions within the heterocycles.

Introduction

Due to their partially filled d orbitals and broad range of oxidation states, transition metals have been used to activate a variety of chemical bonds. In recent years, however, there has been a surge in the use of main-group compounds to activate small molecules in a manner similar to transition metals. Collectively, this field has been recognized as "main-group metallomimetic chemistry".[1–9] At the forefront of these advances is boron, which by virtue of its vacant p_z orbital, is inherently electron deficient.[6,9] Nonetheless, recent developments in boron-based small molecule activation have shown that electron-rich boron systems, such as radicals,[6,10–12] anions,[13–20] and boron–boron multiply bonded systems,[21–29] exhibit a broad array of reactivity toward various small molecules. One of the most commonly utilized methods of boron-based reactivity is through the use of Frustrated Lewis Pairs (FLPs).[30–33]

Since the seminal report by Stephan,[34] FLPs have been used to activate various small molecules, including H_2, CO_2, and NO.[30–33,35] In typical FLPs, sterically bulky functional groups on the Lewis base (LB) and Lewis acid (LA) preclude the formation of typical acid–base adducts, resulting in a formal lone pair on the LB and an empty orbital on the LA. This configuration enables the FLP to act as both an electron donor and acceptor, resembling the frontier d orbitals of transition metals. Accordingly, FLPs have become a key component of main-group "metallomimetic" reactivity and catalysis for various hydrogenation, reduction, and small molecule capture reactions.[30,32,33,36] While traditional FLPs consist of distinct Lewis acidic and basic fragments, recent studies have shown that species with highly strained rings with LB–LA moieties can also react like traditional FLPs.[37–43] Accordingly, a theoretical study by Fernandez demonstrated that the ring-opening reactivity of these cyclic FLPs is dictated by ring strain.[44] Electrochemical transformations of FLPs and their resulting products have been described to result in desired reactivity, including C–F functionalization and metal-free dehydrogenations.[45–50] We hereby report the synthesis of a borinine-based FLP that activates chalcogen-containing small molecules to generate five-membered main-group element heterocycles, as well as the reactivity of these species with potassium graphite or silver(I) trifluoromethanesulfonamide to induce ring expansion.

Results and discussion

Expanding on our previous work to form bis(9-boraphenanthrene),[51,52] and earlier reports by Fukushima,[53] we sought to

[a]*Department of Chemistry, Massachusetts Institute of Technology, 77 Massachusetts Avenue, Building 18-596, Cambridge, MA 02139-4307, USA. E-mail: gilliard@mit.edu*
[b]*Department of Chemistry, University of Virginia, Charlottesville, Virginia 22904, USA*

† Electronic supplementary information (ESI) available: Experimental details, NMR spectra, single-crystal X-ray diffraction data, and computational details. CCDC 2368500–2368507. For ESI and crystallographic data in CIF or other electronic format see DOI: https://doi.org/10.1039/d5sc02000j

‡ These authors contributed equally to this work.

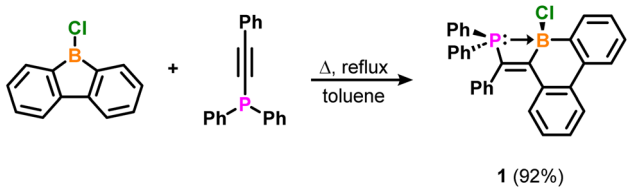

Scheme 1 Synthesis of compound **1** from 9-chloro-9-borafluorene and diphenyl(phenylethynyl)phosphane.

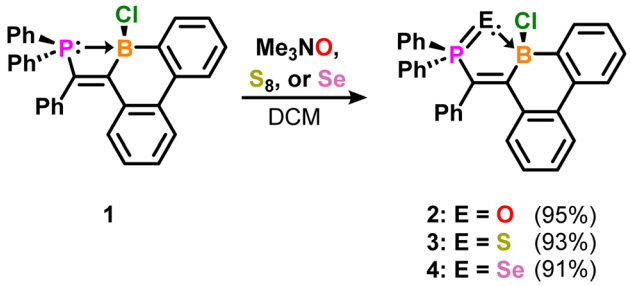

Scheme 2 Ring expansion of compound **1** to form compounds **2–4**.

harness the ring expansion reactivity of 9-chloro-9-borafluorene to form reactive borinines. 9-Chloro-9-borafluorene was reacted with diphenyl(phenylethynyl)phosphane in a 1 : 1 ratio in toluene under reflux conditions (Scheme 1), which led to the isolation of borylphosphinoethylene **1** as an off-white powder in 92% yield. The corresponding $^{11}B\{^1H\}$ resonance appeared at 0.3 ppm as a result of phosphorus-atom coordination to the boron center and is shifted upfield compared to 9-chloro-9-borafluorene (61.5 ppm), consistent with a tetracoordinate boron center.[54] Single crystal X-ray diffraction (SC-XRD) analysis of compound **1** (Fig. 1) reveals that the six-membered boracycle ring is nonplanar due to phosphorus coordination, which forms a four-membered ring (B1–C13–C14–P1). The highly strained nature of the ring is indicated by the P1–C14–C13 angle (95.01(15)°), which is lower than the average for similar B–C–C–P motifs (96.504°, ranging from 94(1)° to 100.6(1)°),[55] as well as the ideal C(sp^2) bond angle of 120°. The B1–P1 bond length (2.018(2) Å) is also shorter than the average reported for similar systems with strained B–P bonds (2.062 Å, ranging from 1.985(1)° to 2.168(2)°).[55]

Because of the highly strained B–P ring, it was hypothesized that the four-membered ring may undergo ring expansion upon reaction with elemental chalcogens to form main-group element-doped five-membered rings, analogous to those previously reported.[37,38,43] With compound **1** in hand, combination of the FLP with trimethylamine *N*-oxide (Me_3N–O), elemental sulfur (S_8), and grey selenium (Se) in dichloromethane (DCM) at room temperature led to the formation of compounds **2**, **3**, and **4**, respectively (Scheme 2). Colorless, plate-shaped crystals of each species were grown in 90% (**2**), 93% (**3**), and 91% (**4**) yields. The $^{11}B\{^1H\}$ NMR spectra of compounds **2**, **3**, and **4** show signals at 10.9, 10.1, and 9.3 ppm, respectively, which are indicative of tetracoordinate boron centers. The $^{31}P\{^1H\}$ NMR peaks are observed at 72.9, 68.2, and 59.3 ppm, respectively, values that differ significantly from their E=PPh_3 counterparts (O=PPh_3: 29.3 ppm, S=PPh_3: 43.2 ppm, Se=PPh_3: 35.8 ppm).[56] The identities of compounds **2–4** were verified *via* SC-XRD analysis (Fig. 2).

The solid-state structures of compounds **2–4** each feature B1–C13–C14–P1–E1 (E = O, S, Se) five-membered planar rings with an out-of-plane chlorine atom bound to the tetrahedral boron center. Relevant interatomic distances and angles are summarized in Fig. 2. As expected, the B1–P1 interatomic distance changes substantially from compound **1** (2.018(2) Å) after ring expansion to form compounds **2–4**, reflecting the influence of the chalcogen size (2.527(3) Å for **2**, 2.876(4) Å for **3**, and 2.965(5) Å for **4**). Because the phosphorus–chalcogen bond distances (1.5433(17) (**2**), 2.0170(10) (**3**), 2.1601(10) Å (**4**)) are all similar to the average C_3P=E bonds (1.495 Å (O), 1.978 Å (S), 2.127 Å (Se)), the P=E interaction is most appropriately described as a double bond. Consequently, the boron–chalcogen interaction is best characterized as a dative interaction. The E→B distances in **2** (1.528(3) Å), **3** (1.968(3) Å), and **4** (2.110(4) Å) align with the average E→B distances reported in the literature (1.517 Å (O), 1.954 Å (S), 2.1670 Å (Se)).[55] Notably, the B1–E1–P1 bond angle decreases as a function of chalcogen size, while the B1–C13–C14 and P1–C14–C13 bond angles each increase.

In an attempt to isolate the intramolecular phosphine-stabilized borinine anion *via* chemical reduction of compounds **2**, **3**, and **4** using 2 equivalents of potassium graphite (KC_8), compounds **5**, **6**, and **7** were obtained from compounds **2**, **3**, and **4**, respectively (Scheme 3, top). Colorless, plate-shaped crystals were obtained after several days in 88% yield for **5**, 91% yield for **6**, and 89% yield for **7**.

The $^{11}B\{^1H\}$ NMR spectra of compounds **5**, **6**, and **7** show signals at 0.7, −14.8, and −17.2 ppm, respectively, consistent with tetracoordinate boron centers. The $^{31}P\{^1H\}$ NMR peaks are observed at 18.1, 10.6, and −4.3 ppm for **5**, **6**, and **7**, respectively. Both the $^{11}B\{^1H\}$ and $^{31}P\{^1H\}$ NMR peaks are shifted upfield compared to those of compounds **2**, **3**, and **4**. When compound **1** was reacted with 1 equivalent of KC_8 in THF, compound **5** was formed *via* THF activation. However, when

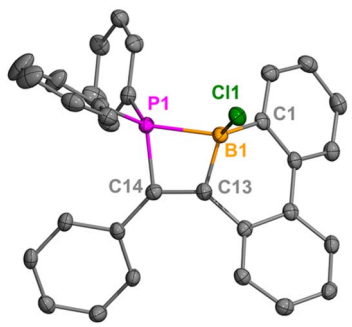

Fig. 1 Molecular structure of **1**; hydrogen atoms are omitted for clarity. Anisotropic displacement parameters are depicted at 50% probability level. Selected distances (Å) and angles (°): B1–P1: 2.018(2); B1–Cl1: 1.885(3); C13–C14: 1.366(3); B1–C13–C14: 107.43(19); P1–C14–C13: 95.01(15)°.

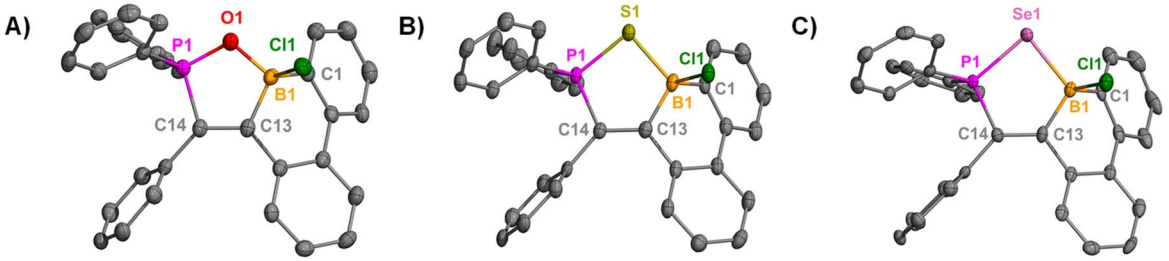

Fig. 2 Molecular structures of **2** (A), **3** (B), and **4** (C); hydrogen atoms are omitted for clarity. Anisotropic displacement parameters are depicted at 50% probability level. Selected distances (Å) and angles (°): **2**: B1–P1: 2.527(3); B1–O1: 1.528(3); B1–Cl1: 1.915(3); P1–O1: 1.5433(17); C13–C14: 1.357(3); B1–C13–C14: 115.1(2); P1–C14–C13: 105.41(17); B1–O1–P1: 110.71(15) **3**: B1–P1: 2.876(4); B1–S1: 1.968(3); B1–Cl1: 1.903(3); P1–S1: 2.0170(10); C13–C14: 1.352(5); B1–C13–C14: 121.0(3); P1–C14–C13: 112.3(2); B1–S1–P1: 92.39(4) **4**: B1–P1: 2.965(5); B1–Se1: 2.110(4); B1–Cl1: 1.902(5); P1–S1: 2.1601(10); C13–C14: 1.349(5); B1–C13–C14: 123.2(3); P1–C14–C13: 113.7(3); B1–Se1–P1: 87.93(12).

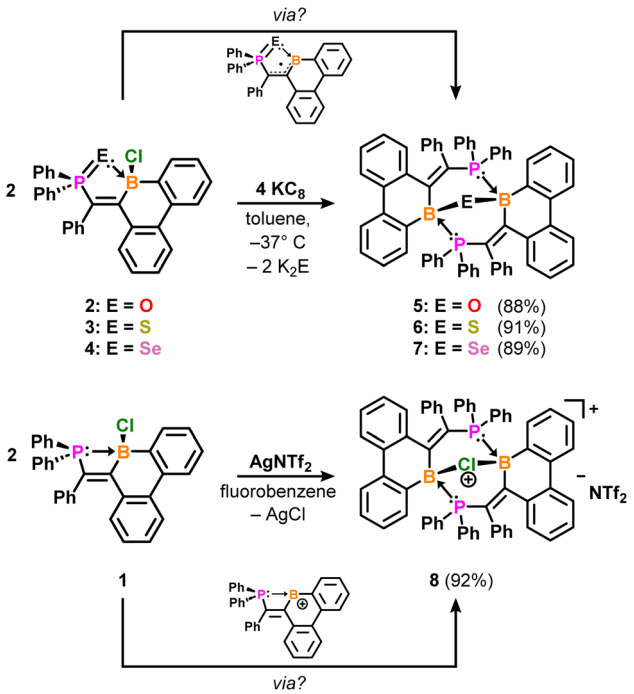

Scheme 3 Synthesis of compounds **5**, **6**, **7** (top) and **8** (bottom).

THF was replaced with toluene, the reaction produced an analogue of compound **1** featuring a B–H bond, likely due to hydrogen abstraction from the solvent (Scheme S1†).

In attempts to form an intramolecular phosphine-stabilized borenium ion, compound **8** was synthesized by combining compound **1** with silver bis(trifluoromethanesulfonyl)imide ($AgNTf_2$) in a 1 : 1 molar ratio in fluorobenzene at room temperature (Scheme 3, bottom). The $^{11}B\{^1H\}$, $^{31}P\{^1H\}$, and ^{19}F NMR signals appear at 3.0, 21.3, and −77.6 ppm, respectively. Notably, the addition of excess $AgNTf_2$ to compound **8** did not result in halide abstraction of the remaining chloride.

Compounds **5–7** were crystalized in a colorless, plate-like form from toluene at −37 °C. All three compounds (**5–7**) adopt a bowl-type geometry, where the phosphorus atoms of one borinine coordinate to the boron center of the other, forming an 8-membered ring with a central μ_2-E (E = O, S, and Se) atom bound to the B atoms (Fig. 3A–C). The B–E–B (E = O, S, and Se) bond angles in **5–7** measure 121.7(3)°, 99.9(3)°, and 95.37(17)°, respectively. The average B–O, B–S, and B–Se bond lengths are 1.436(6), 1.895(10), and 2.041(6) Å, whereas the average B–P bond lengths in **5–7** are 2.078(4), 1.989(10), and 1.983(6) Å, respectively, each within the expected range. From these data, it is observed that when the B–E bond lengths increase, the B–P bond lengths decrease. Although similar dibora-bicyclononane structures with a μ_2–O have been previously reported,[57–65] the μ_2–S (one example)[66] and μ_2–Se (no examples) bonds are exceedingly rare for this motif.

Compound **8** was obtained as yellow, block-like crystals from fluorobenzene at −37 °C, enabling its structural characterization *via* SC-XRD studies. Interestingly, compound **8** exhibits a bonding motif similar to **5–7**, despite markedly different reaction conditions (Fig. 3D). The B1–Cl1 bond length (1.9599(17) Å) is nearly identical to the B2–Cl1 bond distance (1.9548(18) Å), and both exceed the average B–Cl bond length (1.812 Å, ranging from 1.41(4) Å to 2.360(2) Å) reported in the literature.[55] Due to these similarities, compound **8** was subjected to theoretical analysis to understand its electronic structure (*vide infra*). Although other species containing a B–Cl–B bonding motif have been reported, they primarily exist as neutral or anionic species.[67–72] The only known cationic B–Cl–B species were reported by Braunschweig[73] and Chein and Chiu.[74] It should be noted that neither Braunschweig nor Chein and Chiu characterized the bonding interactions between boron and chlorine within their reported species using theoretical methods. Braunschweig's $[B_2Cl_3(IDip)_2]^+$ displays significantly asymmetric B–Cl bonds (1.992(7) Å and 2.257(6) Å), which is the result of one B–Cl covalent interaction and one Cl→B dative interaction. However, the B–Cl bonds in $[B_2Cl_3(IMes)_2]^+$ (2.033(2) Å and 2.078(2) Å) are much more similar to one another. Furthermore, Chein and Chiu's masked borenium ion exhibits symmetric B–Cl bond lengths (1.991(1) Å and 1.990(1) Å), a feature also observed in compound **8**.

With all compounds isolated, density functional theory (DFT) was employed to analyze the electronic structure of compounds **1–4**. Analysis of the Wiberg Bond Indices (WBI) at the B3LYP[75,76]-D3(BJ)[77]/def2-TZVP[78] level of theory indicates that the B–Cl in **1** can be regarded as a single bond ($WBI_{B-Cl} = 0.944$).

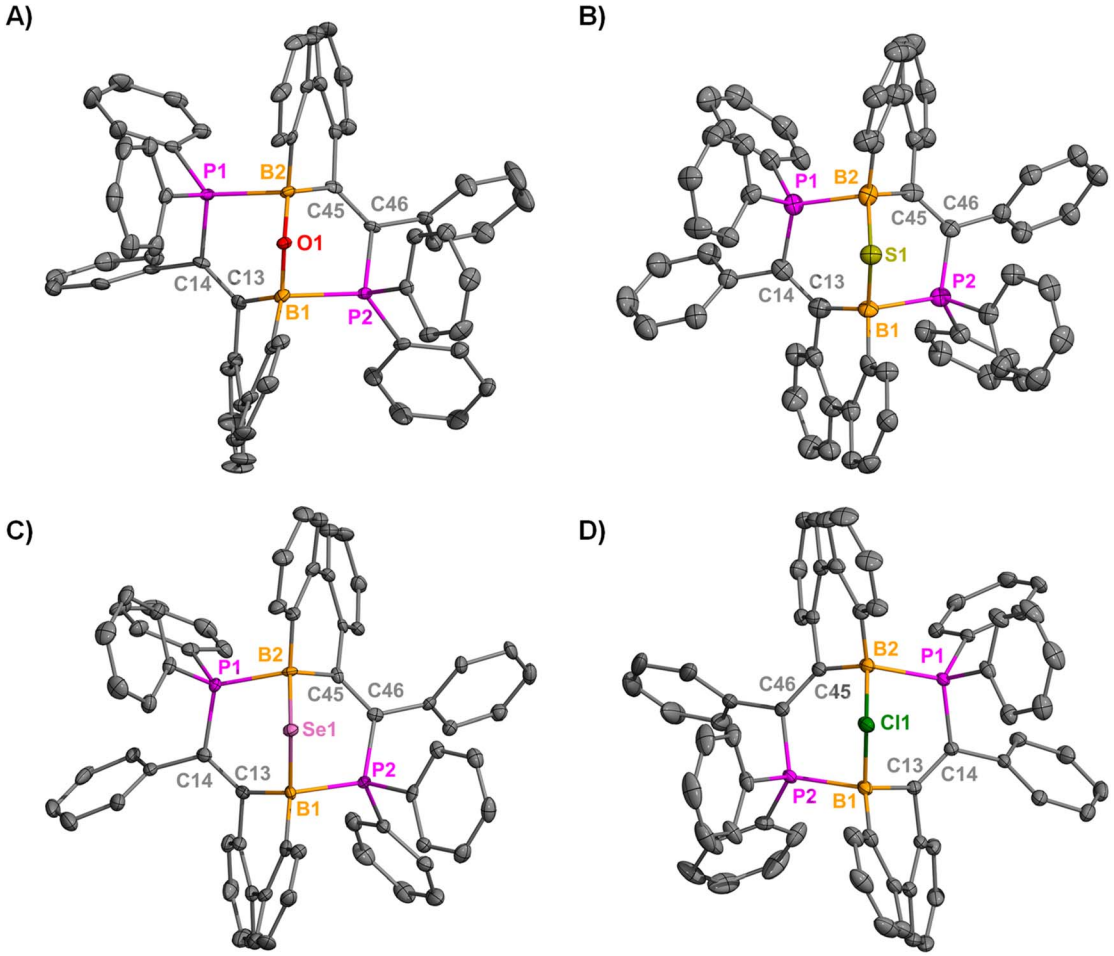

Fig. 3 Molecular structures of **5** (A), **6** (B), **7** (C), and **8** (D); hydrogen atoms, solvents, and counteranions (**8**) are omitted for clarity. Anisotropic displacement parameters are depicted at 50% probability level. Selected distances (Å) and angles (°): **5**: B1–P2: 2.080(4); B1–O1: 1.439(4); B2–P1: 2.075(4); B2–O1: 1.432(4); B1–O1–B2: 121.7(3) **6**: B1–P2: 2.008(6); B1–S1: 1.893(6); B2–P1: 1.996(7); B2–S1: 1.902(7); B1–S1–B2: 99.9(3) **7**: B1–P2: 1.976(4); B1–Se1: 2.035(5); B2–P1: 1.989(5); B2–Se1: 2.035(5); B1–Se1–B2: 95.37(17) **8**: B1–P2: 1.9958(18); B1–Cl1: 1.9599(17); B2–P1: 1.9986(17); B2–Cl1: 1.9548(18); B1–Cl1–B2: 101.30(7).

However, this bond weakens in the case of compound **2** (WBI_{B-Cl} = 0.883), which can be rationalized by enhanced electron density at the boron center, resulting in weaker Cl→B π back-donation. As the chalcogen changes from S to Se, WBI_{B-Cl} remains mostly unchanged (WBI_{B-Cl} = 0.938 for **3**, WBI_{B-Cl} = 0.968 for **4**) and reflects the reduced orbital overlap between B and the heavier chalcogens.

Model systems based on similar scaffolds by Rivard (**A**)[40] and Nikonov (**B**),[38] as well as $(Ph)_3P–BPh_2Cl$, were used as comparison points to the interaction between boron and phosphorus in compound **1**. Representations of all model systems used for theoretical studies are available in Fig. S34.† Localized molecular orbital analysis (Intrinsic Bonding Orbitals, IBOs)[79] and quantum theory of atoms in molecules (QTAIM) analysis describe bonding interactions between the boron and phosphorus atoms of compound **1** and model systems **A**, **B**, and $(Ph)_3P–BPh_2Cl$ (Table S7†). The ρ(B–P) term denotes the electron density at the bond critical point (BCP) between boron and phosphorus, where a lower ρ value indicates a weaker covalent bond. The ρ(B–P) value for compound **1** is significantly lower than that of **A** and **B**, suggesting a more labile B–P bond in compound **1**. Further evidence for the weak B–P bond in **1** is represented by the low H(B–P) value, which represents the total electron density at the BCP. Visualization of contour plots of the Laplacian of electron density for compounds **1**, **A**, **B**, and $(Ph)_3P–BPh_2Cl$ are available in Fig. S35–S38.† The curved nature of the bond paths between the boron and phosphorus atoms in **1**, **A**, and **B** are a result of the strained B–C–C–P ring in each system, while the bond path in $(Ph)_3P–BPh_2Cl$ is linear.

Localized molecular orbital analysis of compounds **2–4** identifies localized bonds displaying a σ bond between E and B, both s and p character between P and E, and a single lone pair on E (Fig. 4 and S39†). To further examine the nature of the E–B bond in compounds **2–4**, energy decomposition analysis in conjunction with the natural orbitals of chemical valence method (EDA-NOCV) was performed to contrast electron-sharing (ES) and donor–acceptor (DA) bonding models. EDA-NOCV results indicate that the E–B bond in compounds **2–4** is best described as a donor–acceptor interaction, in which a lone pair on the chalcogen coordinates to the boron center (Fig. 4B

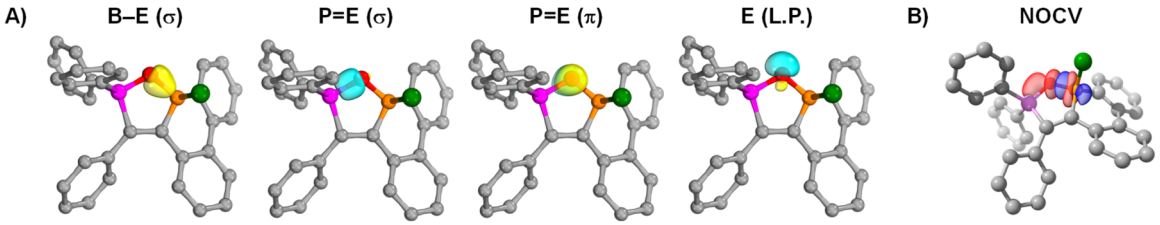

Fig. 4 (A) Intrinsic bonding orbitals (IBOs) of the B–O and P=O (σ and π) bonding interactions, as well as E lone pairs, in compound **2** computed at the B3LYP-D3BJ/def2TZVP level of theory. Orbital iso-surfaces enclose 70% of the integrated electron density of the orbital. (B) NOCV deformation density of the most significant orbital interaction for **2**. Direction of charge migration is red to blue. Hydrogen atoms are omitted for clarity.

and Table S8†). The strength of these E–B dative interactions decrease with the heavier chalcogens (E–B: O; −146 kcal mol^{-1} > S; −125 kcal mol^{-1} > Se; −121 kcal mol^{-1}). Taken together with the experimental SC-XRD data, these computational findings suggest that the phosphorus–chalcogen interaction retains double-bond character, accompanied by a chalcogen–boron dative interaction.

Further insight into the electronic structure of compounds **1–8** was achieved by analyzing their frontier molecular orbitals, computed at the CPCM(DCM)-B3LYP-D3(BJ)//B3LYP-D3(BJ)/def2-TZVP level of theory. In each compound **1–4**, the highest occupied molecular orbital (HOMO) lies primarily on the borinine unit (Fig. S40†). However, notable differences are observed in the lowest unoccupied molecular orbital (LUMO) of these systems. Whereas the LUMO of compound **1** exhibits significant density on the endocyclic alkene carbons, compounds **2–4** have LUMOs that are more localized on the endocyclic alkene carbons, as well as the –PPh$_2$ motif. Comparison of the HOMO of compounds **5–8** indicates that the each HOMO of each system lies on the borinine core, with additional contribution from the bridging chalcogen (O, S, Se for **5**, **6**, **7**, respectively) (Fig. S41†). The LUMO of these systems lies primarily on the endocyclic alkene carbons. Despite the HOMO of compounds **5–7** possessing significant chalcogen non-bonding orbital contribution, the HOMO of compound **8**$^+$ (counter-anion not considered) possesses no Cl lone pair characteristics. Instead, the HOMO of compound **8**$^+$ resembles that of compounds **1–4** by residing primarily on the borinine backbone.

Although compound **8** is formally a cationic species, the nature of the bridging B–Cl–B moiety remains ambiguous due to the potential for both donor–acceptor and electron-sharing bonding interactions. Owing to this ambiguity, a more comprehensive theoretical analysis was conducted to elucidate the nature of the B–Cl–B bond and to assess the possibility of a bridged chloronium species. The Hirshfeld CM-5 charge[80] on the Cl atom in **8**$^+$ was calculated to be +0.210, while the charge on both B atoms is −0.190 (Table 1). For comparison, the CM-5 charges of relevant literature compounds, including the chloroborane borenium ion reported by Chein and Chiu (**C**$^+$),[74] the [B$_2$Cl$_3$(IMes)$_2$] cation reported by Braunschweig[73] (**D**$^+$), **Me$_2$Cl**$^+$ reported by Stoyanov and Reed,[81] and pyCl$^+$ and py$_2$Cl$^+$ reported by Riedel[82] were also computed (Table 1). All species, with the exception of **D**$^+$ (−0.040) and py$_2$Cl$^+$ (+0.080), exhibit a positive Cl atom charge of approximately +0.200, suggesting a chloronium ion. IBO analysis of **8**$^+$ indicates a single covalent interaction between the central chlorine atom and each boron center, identifying two B–Cl σ bonds and two lone pairs (s and p character) on chlorine (Fig. S42†). As observed in diaryliodonium ions theoretically analyzed by Huber and Legault,[83] the s and p lone pairs on chlorine remain localized due to the bent geometry at chlorine, preventing delocalization to either boron center. EDA-NOCV analysis was subsequently performed on **8**$^+$ to compare both donor–acceptor and electron-sharing models for the bridging B–Cl–B moiety. EDA–NOCV results confirm that the most appropriate bonding model is an electron-sharing interaction between two triplet fragments: a chlorine cation and the diboracycle (Fig. S45 and Table S9†). A

Table 1 Computed bond distances and CM5 charges[80] computed at the CPCM-B3LYP-D3BJ/def2TZVP level of theory for compounds **8**$^+$, **C**$^+$, **D**$^+$, **Me$_2$Cl+**, **pyCl**$^+$, and **py$_2$Cl**$^+$. The dielectric constant (ε) was set to 5.42 to resemble fluorobenzene solvation

Compound	*r*(B–Cl) (Å)	CM5(B)	CM5(Cl)
8$^+$	1.963	−0.19	+0.21
C$^+$	2.020	+0.01	+0.16
D$^+$	1.830 (exocyclic)	−0.15	−0.04 (exocyclic)
	2.043 (endocyclic)	—	+0.07 (endocyclic)
Me$_2$Cl$^+$	—	—	+0.32
pyCl$^+$	—	—	+0.22
py$_2$Cl$^+$	—	—	+0.08

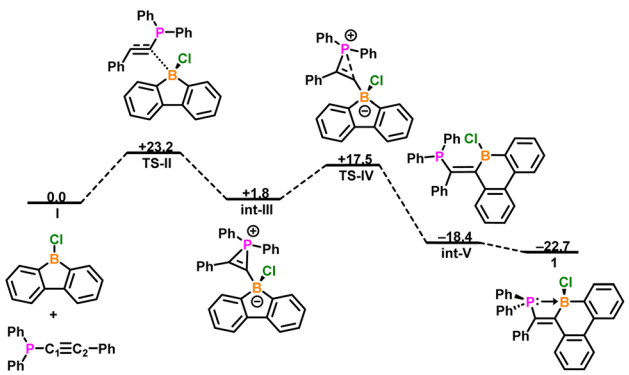

Fig. 5 Calculated relative gas-phase free energies (Δ*G*, kcal mol^{-1}) for the reaction between 9-chloro-9-borafluorene and diphenyl(phenylethynyl)phosphane to form compound **1** computed at the B3LYP-D3(BJ)/def2-TZVP level of theory.

qualitative molecular orbital diagram for the B–Cl–B bonding interactions, including the relevant localized bonding orbitals, is provided in Fig. S42.† These combined theoretical results unambiguously identify the chlorine in compound **8** as a chloronium ion, representing one of the earliest examples of such a species supported by two boron centers.

The mechanism to form boracyclohexadienes from 9-chloro-9-borafluorene has been previously reported by Braunschweig and Lin.[84] Drawing inspiration from this study, density functional theory was employed to investigate a possible mechanism for the formation of compound **1** at the B3LYP-D3(BJ)/def2-TZVP level of theory (Fig. 5). Starting from **I**, the C_1 carbon of diphenyl(phenylethynyl)phosphane acts as a nucleophile and attacks the boron center (**TS-II**, $\Delta G^{\ddagger}$ = +23.2 kcal mol^{-1}), resulting in formation of **int-III** ($\Delta\Delta G$ = −20.0 kcal mol^{-1}), in which a phosphirenium ion and borafluorenate are formed. Through **TS-IV** ($\Delta\Delta G^{\ddagger}$ = +15.8 kcal mol^{-1}), the phosphirenium ring opens, resulting in a 1,2-shift of the diphenylphosphino group to the C_2 carbon, as well as ring expansion of the borafluorene to form borinine **int-V** ($\Delta\Delta G$ = −35.9 kcal mol^{-1}). The diphenylphosphino moiety then rotates to form compound **1** ($\Delta\Delta G$ = −4.3 kcal mol^{-1}).

The second mechanism of interest involves the reductive ring expansion of compound **2** to form compound **5**. A proposed mechanism for this process was computed at the B3LYP-D3(BJ)/def2-TZVP level of theory (Fig. 6). Addition of potassium metal to compound **2** results in the formation of **int-A** (ΔG = −22.6 kcal mol^{-1}), in which the potassium atom is stabilized by the π-system of a neighboring phosphine ring and the central oxygen ring. From **int-A**, KCl leaves the coordination sphere of the reduced heterocycle (**int-B**, $\Delta\Delta G$ = −8.1 kcal mol^{-1}), subsequently forming **int-C** ($\Delta\Delta G$ = +10.8 kcal mol^{-1}), which suggests the formation of a phosphine-stabilized boryl radical. A second equivalent of **int-C** combines to produce the open-shell singlet **int-D** ($\Delta\Delta G$ = −7.9 kcal mol^{-1}), in which the two **int-C** units are in close proximity to each other. A radical coupling transition state (**TS-E**, $\Delta\Delta G^{\ddagger}$ = +27.7 kcal mol^{-1}) from **int-D** was found to be the rate determining step of the mechanism. Once the bridging oxygen–boron bond is formed, the newly generated system becomes a closed-shell singlet (**int-F**, $\Delta\Delta G$ = −47.2 kcal mol^{-1}). Subsequent addition of two equivalents of potassium metal results in the dipotassium species **int-H** ($\Delta\Delta G$ = −27.4 kcal mol^{-1}). Loss of K_2O from **int-H** leads to the ring-expanded compound **5** (ΔG = −87.1 kcal mol^{-1}). To

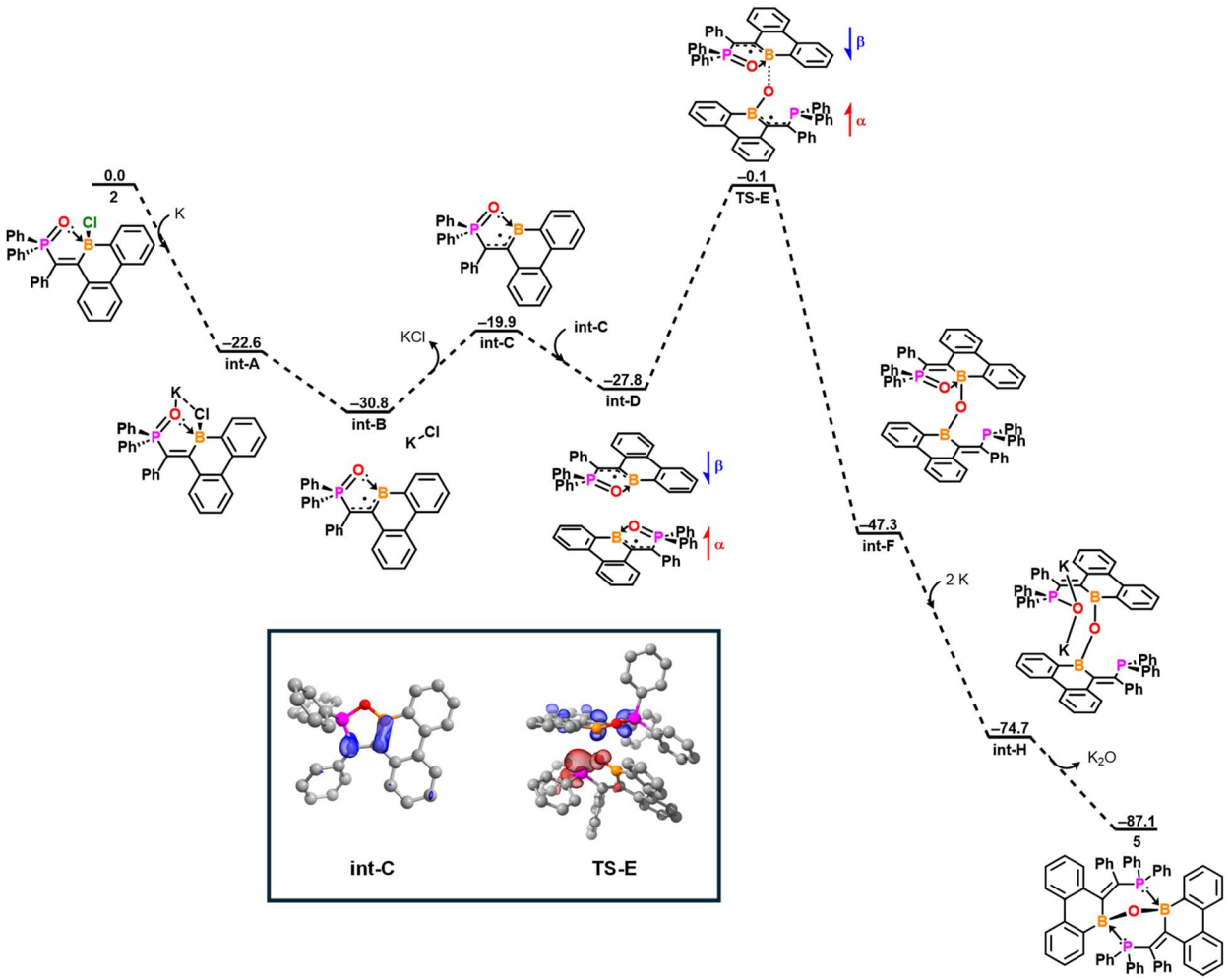

Fig. 6 Calculated relative gas-phase free energies (Δ*G*, kcal mol^{-1}) for reduction and subsequent ring expansion of compound **2** to form compound **5** computed at the B3LYP-D3(BJ)/def2-TZVP level of theory.

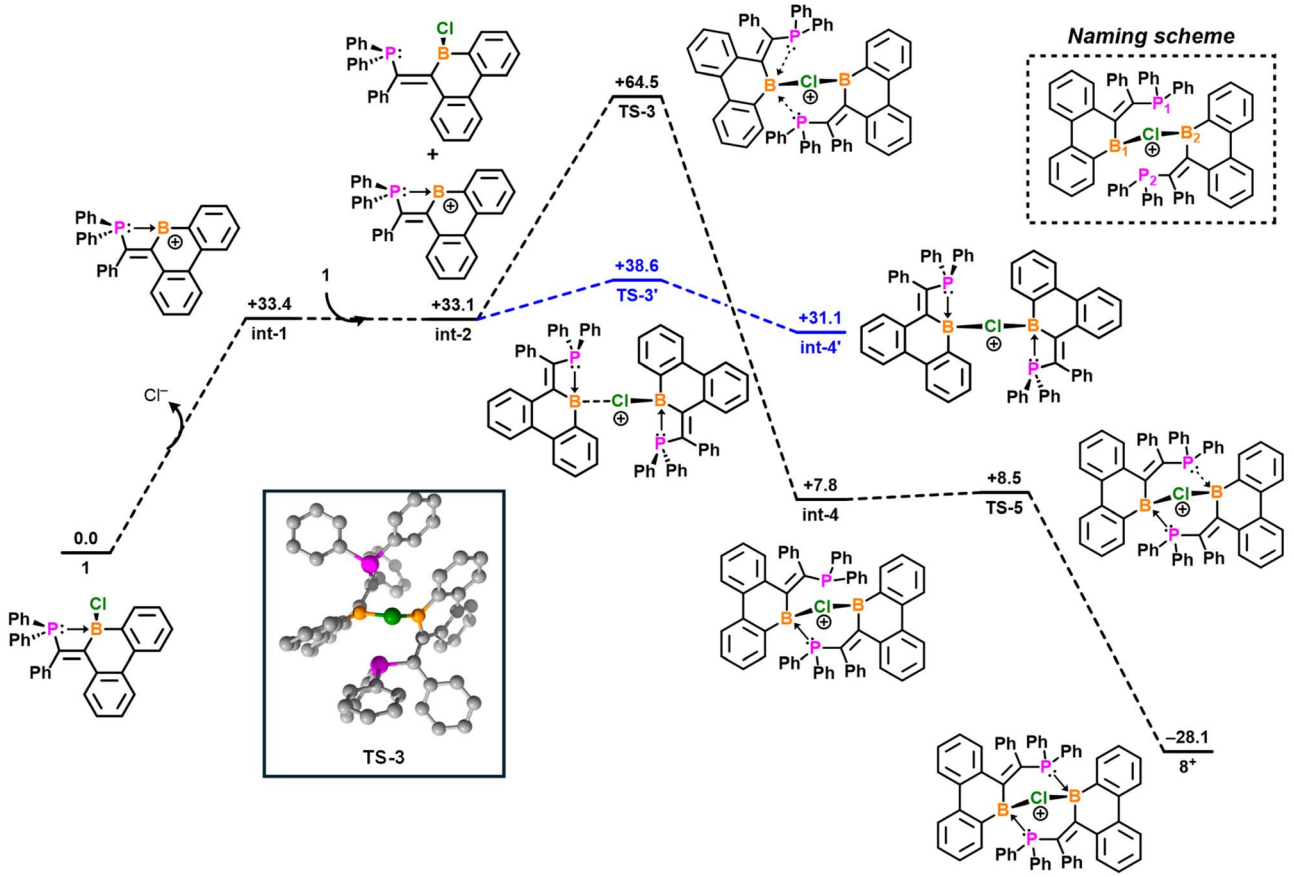

Fig. 7 Calculated relative free energies (ΔG, kcal mol^{-1}) for halide abstraction and subsequent ring expansion of compound **1** to form compound **8**$^{+}$ computed at the CPCM-B3LYP-D3-(BJ)/def2-TZVP level of theory. The dielectric constant (ε) was set to 5.42 to resemble fluorobenzene solvation.

account for the formation of solid K_2O, the computed ΔG_{rxn} from **int-H** to compound **5** was adjusted by adding the experimental $\Delta G_{deposition}$ for KCl (−55.7 kcal mol^{-1}) to the computed ΔG_{rxn}. Despite our best efforts to model the potential energy surface for S and Se analogues, **TS-E** could not be located for either system. Nonetheless, we postulate that compounds **3** and **4** proceed through a similar mechanism as compound **2**. The computed intermediates for formation of compounds **6** and **7** are available in Fig. S43 and S44.†

We then sought to propose a mechanism for the ring expansion of compound **1** to form compound **8** upon halide abstraction (Fig. 7). The mechanism begins with the removal of Cl^- from **1**, resulting in the phosphine-stabilized borenium ion **int-1** (ΔG = +33.4 kcal mol^{-1}). Subsequent addition of a second equivalent of **1** forms **int-2** ($\Delta\Delta G$ = −0.3 kcal mol^{-1}). **TS-3** is the result of nucleophilic phosphine attack of P_2 on B_1 in an S_{N_2} fashion ($\Delta\Delta G^{\ddagger}$ = +31.4 kcal mol^{-1}), resulting in dissociation of P_1 from B_1, forming **int-4** (ΔG = −25.3 kcal mol^{-1}). From **int-4**, nucleophilic attack of B_2 by P_1 *via* **TS-5** ($\Delta\Delta G^{\ddagger}$ = +0.7 kcal mol^{-1}), results in the formation of **8**$^{+}$ ($\Delta\Delta G$ = −36.6 kcal mol^{-1}). An alternative low-lying transition state (**TS-3′**), arising from chlorine nucleophilic attack at one of the boron sites ($\Delta\Delta G^{\ddagger}$ = +5.5 kcal mol^{-1}), was also found and results in the ring-closed **int-4′** ($\Delta\Delta G$ = −7.5 kcal mol^{-1}). However, this kinetic product readily reverts to **int-2**, whereas **int-4** provides a significant thermodynamic sink that minimizes reversibility at room temperature.

Conclusions

In summary, we report a new approach to expand the borole ring in 9-chloro-9-borafluorene using diphenyl(phenylethynyl) phosphane to yield a six-membered borinine ring that contains a four-membered B–P heterocycle (**1**). The computed mechanism for the ring expansion shows that the reaction proceeds through a 1,2-shift of the –PPh_2 group. Compound **1** was then used to activate chalcogen sources (Me_3N–O, S_8, and Se) to form five-membered B–E–P heterocycles **2–4**. Subsequent reduction of these species with KC_8 results in K_2E formation, thereby forming an eight-membered ring with a μ_2-chalcogenide connecting two boron centers in compounds **5–7**. A proposed mechanism shows that the rate-determining step of this reductive ring expansion is an open-shell singlet transition state, in which an intermolecular B–E bond is formed. Halide abstraction of compound **1** using silver bis(trifluoromethanesulfonyl)imide forms a proposed intermediate phosphine-stabilized borenium ion, which then ring expands to form compound **8**. Using theoretical methods, we have assigned

compound **8** as containing one of the first examples of a boron-stabilized chloronium ion.

Data availability

Crystallographic data for **1–8** can be found in the Cambridge Crystallographic Database (CCDC: 2368500–2368507). All other data have been provided in the ESI,† including experimental details, NMR spectra, single-crystal X-ray diffraction data, and computational details.

Author contributions

The manuscript was written through contributions of all authors. All authors have given approval to the final version of the manuscript.

Conflicts of interest

There are no conflicts to declare.

Acknowledgements

We are grateful to the National Science Foundation Chemical Synthesis (CHE 2046544) and Major Research Instrumentation (CHE 2018870) programs for support of this work. We also thank the Alfred P. Sloan Foundation for a Sloan Research Fellowship. R. J. G. acknowledges additional laboratory support through a Beckman Young Investigator award from the Arnold & Mabel Beckman Foundation. N. C. F. acknowledges the National Science Foundation for a Graduate Research Fellowship (grant #1842490). N. C. F. thanks Professor Charles Edwin Webster for insightful conversations concerning the computational portions of the paper. The authors acknowledge the MIT SuperCloud and Lincoln Laboratory Supercomputing Center for providing resources that have contributed to the research results reported within this paper/report.

Notes and references

1 Z. Liu, Z. Wang, H. Mu, Y. Zhou, J. Zhou and Z. Dong, *Nat. Commun.*, 2024, **15**, 9849.
2 M. Shibuya, M. Matsuda and Y. Yamamoto, *Chem.–Eur. J.*, 2021, **27**, 8822–8831.
3 S. Bonfante, C. Lorber, J. M. Lynam, A. Simonneau and J. M. Slattery, *J. Am. Chem. Soc.*, 2024, **146**, 2005–2014.
4 A. Gärtner, U. S. Karaca, M. Rang, M. Heinz, P. D. Engel, I. Krummenacher, M. Arrowsmith, A. Hermann, A. Matler, A. Rempel, R. Witte, H. Braunschweig, M. C. Holthausen and M.-A. Légaré, *J. Am. Chem. Soc.*, 2023, **145**, 8231–8241.
5 K. Chulsky, I. Malahov, D. Bawari and R. Dobrovetsky, *J. Am. Chem. Soc.*, 2023, **145**, 3786–3794.
6 M.-A. Légaré, C. Pranckevicius and H. Braunschweig, *Chem. Rev.*, 2019, **119**, 8231–8261.
7 M.-A. Légaré, G. Bélanger-Chabot, R. D. Dewhurst, E. Welz, I. Krummenacher, B. Engels and H. Braunschweig, *Science*, 2018, **359**, 896–900.
8 H. Braunschweig, I. Krummenacher, M.-A. Légaré, A. Matler, K. Radacki and Q. Ye, *J. Am. Chem. Soc.*, 2017, **139**, 1802–1805.
9 Y. Su and R. Kinjo, *Chem. Soc. Rev.*, 2019, **48**, 3613–3659.
10 Y. Su and R. Kinjo, *Coord. Chem. Rev.*, 2017, **352**, 346–378.
11 L. Kong and C. Cui, *Synlett*, 2021, **32**, 1316–1322.
12 N. C. Frey, K. K. Hollister, P. Müller, D. A. Dickie, C. E. Webster and R. J. Gilliard Jr, *Inorg. Chem.*, 2024, **63**, 17639–17650.
13 M. Yamashita and K. Nozaki, *Bull. Chem. Soc. Jpn.*, 2008, **81**, 1377–1392.
14 M. Yamashita and K. Nozaki, in *Synthesis and Application of Organoboron Compounds*, ed. E. Fernández and A. Whiting, Springer International Publishing, Cham, 2015, pp. 1–37, DOI: **10.1007/978-3-319-13054-5_1**.
15 M. Yamashita and K. Nozaki, *Pure Appl. Chem.*, 2008, **80**, 1187–1194.
16 K. E. Wentz, A. Molino, L. A. Freeman, D. A. Dickie, D. J. D. Wilson and R. J. Gilliard Jr, *J. Am. Chem. Soc.*, 2022, **144**, 16276–16281.
17 K. E. Wentz, A. Molino, L. A. Freeman, D. A. Dickie, D. J. D. Wilson and R. J. Gilliard Jr, *Inorg. Chem.*, 2022, **61**, 17049–17058.
18 K. E. Wentz, A. Molino, L. A. Freeman, D. A. Dickie, D. J. D. Wilson and R. J. Gilliard Jr, *Angew. Chem., Int. Ed.*, 2023, **62**, e202215772.
19 K. E. Wentz, A. Molino, S. L. Weisflog, A. Kaur, D. A. Dickie, D. J. D. Wilson and R. J. Gilliard Jr, *Angew. Chem., Int. Ed.*, 2021, **60**, 13065–13072.
20 K. E. Wentz, A. Molino, L. A. Freeman, D. A. Dickie, D. J. D. Wilson and R. J. Gilliard Jr, *Inorg. Chem.*, 2021, **60**, 13941–13949.
21 L. Englert, U. Schmidt, M. Dömling, M. Passargus, T. E. Stennett, A. Hermann, M. Arrowsmith, M. Härterich, J. Müssig, A. Phillipps, D. Prieschl, A. Rempel, F. Rohm, K. Radacki, F. Schorr, T. Thiess, J. O. C. Jiménez-Halla and H. Braunschweig, *Chem. Sci.*, 2021, **12**, 9506–9515.
22 S. R. Wang, M. Arrowsmith, J. Böhnke, H. Braunschweig, T. Dellermann, R. D. Dewhurst, H. Kelch, I. Krummenacher, J. D. Mattock, J. H. Müssig, T. Thiess, A. Vargas and J. Zhang, *Angew. Chem., Int. Ed.*, 2017, **56**, 8009–8013.
23 T. E. Stennett, J. D. Mattock, L. Pentecost, A. Vargas and H. Braunschweig, *Angew. Chem., Int. Ed.*, 2018, **57**, 15276–15281.
24 M. Arrowsmith, J. Böhnke, H. Braunschweig and M. A. Celik, *Angew. Chem., Int. Ed.*, 2017, **56**, 14287–14292.
25 H. Braunschweig, T. Dellermann, W. C. Ewing, T. Kramer, C. Schneider and S. Ullrich, *Angew. Chem., Int. Ed.*, 2015, **54**, 10271–10275.
26 T. Brückner, M. Arrowsmith, M. Heß, K. Hammond, M. Müller and H. Braunschweig, *Chem. Commun.*, 2019, **55**, 6700–6703.
27 J. Böhnke, T. Brückner, A. Hermann, O. F. González-Belman, M. Arrowsmith, J. O. C. Jiménez-Halla and H. Braunschweig, *Chem. Sci.*, 2018, **9**, 5354–5359.

28 T. Matsubara, R. Yamasaki, T. Hori and M. Morikubo, *Bull. Chem. Soc. Jpn.*, 2018, **91**, 1683–1690.
29 H. Braunschweig, P. Constantinidis, T. Dellermann, W. C. Ewing, I. Fischer, M. Hess, F. R. Knight, A. Rempel, C. Schneider, S. Ullrich, A. Vargas and J. D. Woollins, *Angew. Chem., Int. Ed.*, 2016, **55**, 5606–5609.
30 D. W. Stephan, *J. Am. Chem. Soc.*, 2015, **137**, 10018–10032.
31 N. Li and W.-X. Zhang, *Chin. J. Chem.*, 2020, **38**, 1360–1370.
32 D. W. Stephan, *Acc. Chem. Res.*, 2015, **48**, 306–316.
33 D. W. Stephan and G. Erker, *Angew. Chem., Int. Ed.*, 2015, **54**, 6400–6441.
34 G. C. Welch, R. R. S. Juan, J. D. Masuda and D. W. Stephan, *Science*, 2006, **314**, 1124–1126.
35 T. Wang, C. G. Daniliuc, G. Kehr and G. Erker, in *Frustrated Lewis Pairs*, 2021, ch. 3, pp. 87–112, DOI: **10.1007/978-3-030-58888-5_3**.
36 B. L. Frenette and E. Rivard, *Chem.–Eur. J.*, 2023, **29**, e202302332.
37 A. S. Balueva, Y. Y. Efremov, V. M. Nekhoroshkov and O. A. Erastov, *Bulletin of the Academy of Sciences of the USSR*, Division of Chemical Science, 1989, vol. 38, pp. 2557–2560.
38 A. S. Balueva and G. N. Nikonov, *Russ. Chem. Bull.*, 1993, **42**, 341–343.
39 S. Bontemps, M. Devillard, S. Mallet-Ladeira, G. Bouhadir, K. Miqueu and D. Bourissou, *Inorg. Chem.*, 2013, **52**, 4714–4720.
40 A. A. Omaña, R. K. Green, R. Kobayashi, Y. He, E. R. Antoniuk, M. J. Ferguson, Y. Zhou, J. G. C. Veinot, T. Iwamoto, A. Brown and E. Rivard, *Angew. Chem., Int. Ed.*, 2021, **60**, 228–231.
41 V. K. Greenacre, M. B. Ansell, S. M. Roe and I. R. Crossley, *Eur. J. Inorg. Chem.*, 2014, **2014**, 5053–5062.
42 R. Liedtke, C. Eller, C. G. Daniliuc, K. Williams, T. H. Warren, M. Tesch, A. Studer, G. Kehr and G. Erker, *Organometallics*, 2016, **35**, 55–61.
43 S. Porcel, G. Bouhadir, N. Saffon, L. Maron and D. Bourissou, *Angew. Chem., Int. Ed.*, 2010, **49**, 6186–6189.
44 S. Portela and I. Fernández, *Z. Anorg. Allg. Chem.*, 2023, **649**, e202200384.
45 E. J. Lawrence, V. S. Oganesyan, D. L. Hughes, A. E. Ashley and G. G. Wildgoose, *J. Am. Chem. Soc.*, 2014, **136**, 6031–6036.
46 E. J. Lawrence, E. R. Clark, L. D. Curless, J. M. Courtney, R. J. Blagg, M. J. Ingleson and G. G. Wildgoose, *Chem. Sci.*, 2016, **7**, 2537–2543.
47 E. J. Lawrence, T. J. Herrington, A. E. Ashley and G. G. Wildgoose, *Angew. Chem., Int. Ed.*, 2014, **53**, 9922–9925.
48 G.-Q. Chen, G. Kehr, C. G. Daniliuc, M. Bursch, S. Grimme and G. Erker, *Chem.–Eur. J.*, 2017, **23**, 4723–4729.
49 D. Mandal, R. Gupta, A. K. Jaiswal and R. D. Young, *J. Am. Chem. Soc.*, 2020, **142**, 2572–2578.
50 L. J. C. van der Zee, J. Hofman, J. M. van Gaalen and J. C. Slootweg, *Chem. Soc. Rev.*, 2024, **53**, 4862–4876.
51 K. K. Hollister, K. E. Wentz and R. J. Gilliard Jr, *Acc. Chem. Res.*, 2024, **57**, 1510–1522.
52 S. K. Sarkar, K. K. Hollister, A. Molino, A. D. Obi, C.-L. Deng, B. Y. E. Tra, B. M. Stewart, D. A. Dickie, D. J. D. Wilson and R. J. Gilliard Jr, *J. Am. Chem. Soc.*, 2023, **145**, 21475–21482.
53 Y. Shoji, N. Tanaka, S. Muranaka, N. Shigeno, H. Sugiyama, K. Takenouchi, F. Hajjaj and T. Fukushima, *Nat. Commun.*, 2016, **7**, 12704.
54 H. Nöth and B. Wrackmeyer, *Nuclear Magnetic Resonance Spectroscopy of Boron Compounds*, Springer, Berlin, Heidelberg, 1978.
55 C. R. Groom, I. J. Bruno, M. P. Lightfoot and S. C. Ward, *Acta Crystallogr., Sect. B*, 2016, **72**, 171–179.
56 T. A. Albright, W. J. Freeman and E. E. Schweizer, *J. Org. Chem.*, 1975, **40**, 3437–3441.
57 Y. Zhang, M. Li, S. Chandrasekaran, X. Gao, X. Fang, H.-W. Lee, K. Hardcastle, J. Yang and B. Wang, *Tetrahedron*, 2007, **63**, 3287–3292.
58 L. C. Wilkins, J. R. Lawson, P. Wieneke, F. Rominger, A. S. K. Hashmi, M. M. Hansmann and R. L. Melen, *Chem.–Eur. J.*, 2016, **22**, 14618–14624.
59 Q. Wu, M. Esteghamatian, N.-X. Hu, Z. Popovic, G. Enright, S. R. Breeze and S. Wang, *Angew. Chem., Int. Ed.*, 1999, **38**, 985–988.
60 V. Subramaniyan and G. Mani, *Organometallics*, 2018, **37**, 127–135.
61 D. Kanichar, L. Roppiyakuda, E. Kosmowska, M. A. Faust, K. P. Tran, F. Chow, E. Buglo, M. P. Groziak, E. A. Sarina, M. M. Olmstead, I. Silva and H. H. Xu, *Chem. Biodiversity*, 2014, **11**, 1381–1397.
62 R. Köster, A. Sporzyński, W. Schüßler, D. Bläser and R. Boese, *Chem. Ber.*, 1994, **127**, 1191–1199.
63 A. Torres-Huerta, M. d. J. Velásquez-Hernández, L. G. Ramírez-Palma, F. Cortés-Guzmán, D. Martínez-Otero, U. Hernández-Balderas and V. Jancik, *Inorg. Chem.*, 2017, **56**, 10032–10043.
64 J.-H. Son, S. R. Tamang, J. C. Yarbrough and J. D. Hoefelmeyer, *Z. Naturforsch., B*, 2015, **70**, 775–781.
65 D. Zhu, J. H. W. LaFortune, R. L. Melen and D. W. Stephan, *Dalton Trans.*, 2019, **48**, 2038–2045.
66 N. Schulenberg, O. Ciobanu, E. Kaifer, H. Wadepohl and H.-J. Himmel, *Eur. J. Inorg. Chem.*, 2010, **2010**, 5201–5210.
67 H. E. Katz, *Organometallics*, 1987, **6**, 1134–1136.
68 S. P. Lewis, N. J. Taylor, W. E. Piers and S. Collins, *J. Am. Chem. Soc.*, 2003, **125**, 14686–14687.
69 K. Samigullin, I. Georg, M. Bolte, H.-W. Lerner and M. Wagner, *Chem.–Eur. J.*, 2016, **22**, 3478–3484.
70 A. Kobayashi, K. Suzuki, R. Kitamura and M. Yamashita, *Organometallics*, 2020, **39**, 383–387.
71 M. J. Sgro, J. Dömer and D. W. Stephan, *Chem. Commun.*, 2012, **48**, 7253–7255.
72 H. Braunschweig, A. Damme, R. D. Dewhurst, T. Kramer, T. Kupfer, K. Radacki, E. Siedler, A. Trumpp, K. Wagner and C. Werner, *J. Am. Chem. Soc.*, 2013, **135**, 8702–8707.
73 L. Englert, A. Stoy, M. Arrowsmith, J. H. Muessig, M. Thaler, A. Deißenberger, A. Häfner, J. Böhnke, F. Hupp, J. Seufert, J. Mies, A. Damme, T. Dellermann, K. Hammond, T. Kupfer, K. Radacki, T. Thiess and H. Braunschweig, *Chem.–Eur. J.*, 2019, **25**, 8612–8622.

74 D.-N. Shih, R. Boobalan, Y.-H. Liu, R.-J. Chein and C.-W. Chiu, *Inorg. Chem.*, 2021, **60**, 16266–16272.
75 A. D. Becke, *J. Chem. Phys.*, 1993, **98**, 5648–5652.
76 C. Lee, W. Yang and R. G. Parr, *Phys. Rev. B*, 1988, **37**, 785–789.
77 S. Grimme, S. Ehrlich and L. Goerigk, *J. Comput. Chem.*, 2011, **32**, 1456–1465.
78 F. Weigend and R. Ahlrichs, *Phys. Chem. Chem. Phys.*, 2005, **7**, 3297–3305.
79 G. Knizia, *J. Chem. Theory Comput.*, 2013, **9**, 4834–4843.
80 A. V. Marenich, S. V. Jerome, C. J. Cramer and D. G. Truhlar, *J. Chem. Theory Comput.*, 2012, **8**, 527–541.
81 E. S. Stoyanov, I. V. Stoyanova, F. S. Tham and C. A. Reed, *J. Am. Chem. Soc.*, 2010, **132**, 4062–4063.
82 P. Pröhm, W. Berg, S. M. Rupf, C. Müller and S. Riedel, *Chem. Sci.*, 2023, **14**, 2325–2329.
83 R. Robidas, D. L. Reinhard, S. M. Huber and C. Y. Legault, *Chemphyschem*, 2023, **24**, e202200634.
84 Z. Wang, Y. Zhou, J.-X. Zhang, I. Krummenacher, H. Braunschweig and Z. Lin, *Chem.–Eur. J.*, 2018, **24**, 9612–9621.